Chemical Engineering Journal 142 (2008) 225–238

Contents lists available at ScienceDirect

Chemical Engineering Journal

journal homepage: www.elsevier.com/locate/cej

Review

Interactions between reaction kinetics in ATR-reactors and transport mechanisms in functional ceramic membranes: A simulation approach

Jens Hüppmeier*, Michael Baune, Jorg Thöming

Center for Environmental Research and Technology, University of Bremen, Leobener Straße UFT, 28359 Bremen, Germany

ARTICLE INFO

Article history:
Received 12 December 2007
Received in revised form 29 February 2008
Accepted 3 March 2008

Keywords:
Autothermal reforming
Hot-spot minimization
Palladium
Hydrogen membrane

ABSTRACT

In this investigation the interaction between the mass transport in separation membranes and the autothermal steam-reforming in a membrane reactor was studied with a special focus on the consequences for designing smart materials that influence the reactor performance. A steady-state 1D-model was used to determine optimal thicknesses of Pd/Ag-layers for separating hydrogen gas from the reactor. The results indicate that a 400 nm layer is optimal for reactor temperatures ranging from 450 to 600 °C. To attain ideal isothermal reaction conditions, a spatial dynamic model containing an oxygen feeding controller was employed. It showed that depending proportionality of temperature with a small differential part, a controller is best suited for minimize deviations from the isothermal behaviour. In this work, an oxygen flux characteristic of the controller was used to simulate a functionalized membrane with the same characteristic. The obtained results are almost as good as in the ideal case with values up to 99% reaction yield at 600 °C in a 100 mm tube reactor.

1. Introduction

Fuel cell technology has gained significant interest in recent years because of its high energy density and low operating temperatures [1,2] and is very suitable for future electrical power generation with a great potential for small scale applications in electronic and electrical equipment such as notebooks or automotives. As a representative, polymer electrolyte membrane (PEM) fuel cell is a candidate to satisfy both prerequisites, but directly needs hydrogen gas with high purities or low contamination of harmful gases like carbon monoxide. Because of many difficulties in hydrogen gas storage and distribution, it can be produced alternatively on-board in a micro-reactor located upstream of the fuel cell from easily available and storable fuels like methane, propane or butane. In this report we focus on methane as fuel, for which reaction kinetics of autothermal reforming is well known.

The autothermal reforming (ATR) is a concept of producing hydrogen with increasing interest in research and industry [2–7]. It is essentially a combination of endothermic steam-reforming (SR) process chemically expressed as

$$CH_4 + H_2O \leftrightarrow CO + 3\,H_2 \quad (\Delta H_R^0 = 206(\mathrm{kJ/mol}))$$

and the exothermic partial oxidation (PO) written as

$$CH_4 + 0.5\,O_2 \rightarrow CO + 2\,H_2 \quad (\Delta H_R^0 = -36(\mathrm{kJ/mol}))$$

both of which are themselves concepts of producing hydrogen gas. These reactions are completed with a third exothermic reaction referred to as the water-gas-shift (WGS) with a formulation

$$CO + H_2O \leftrightarrow CO_2 + H_2 \quad (\Delta H_R^0 = -41(\mathrm{kJ/mol})).$$

After a short contact time, all three reactions reach thermodynamic equilibrium.

Based upon theoretical calculations and through verification from many experiments, it has been established that the ATR combines the advantages of the two hydrogen producing concepts, with negligible disadvantages [3–5] like additional heating or cooling of the reactor. Moreover, because of prior experience in industrial applications, much work was done to improve the design and the performance of ATR-reactors.

In this investigation a concept for the separation of hydrogen during reaction by means of a highly selective membrane, for example dense Pd-membranes that allow purities of hydrogen of up to 99.99% [9], so as to enable a direct feed to the PEM fuel cells is proposed. Furthermore, by removing one product from the equilibrium, higher conversion rates with respect to hydrogen production can be expected. This enhances the WGS reaction [3,5,8] therefore increasing the overall hydrogen gas yield. This equilibrium shifting supports also the reforming reaction as well

* Corresponding author. Tel.: +49 421 218 63386.
E-mail address: jhuepp@uni-bremen.de (J. Hüppmeier).

1385-8947/$ – see front matter © 2008 Elsevier B.V. All rights reserved.
doi:10.1016/j.cej.2008.03.004

Nomenclature

B_0	permeability constant (m^2)
c	heat capacity ($kJ\,kg^{-1}\,K^{-1}$)
d	thickness, diameter (m)
d_H	hydraulical diameter (m)
D	reactor diameter (m)
D_{i,H_2}	diffusion coefficient ($m^2\,s^{-1}$)
D_R	diameter of the reactor (m)
E	activation energy ($kJ\,mol^{-1}$)
ΔG	molar reaction free enthalpy ($kJ\,mol^{-1}$)
ΔH	molar reaction enthalpy ($kJ\,mol^{-1}$)
J	area-specific molar flux ($mol\,s^{-1}\,m^{-2}$)
k	reaction rate constant
K_{eq}	equilibrium constant
K^{OX}	adsorption constant (bar^{-1})
K_0	Knudson coefficient (m)
L	reactor length (m)
M_i	molar mass ($g\,mol^{-1}$)
n	Sievert's law exponent
p	pressure (Pa)
Q	permeability ($mol\,m^{-1}\,s^{-1}\,Pa^{-n)}$
r	reaction rate ($mol\,kg^{-1}\,s^{-1}$)
R	molar gas constant ($J\,mol^{-1}\,K^{-1}$)
t	time (s)
T	over-all temperature (K)
u	gas velocity ($m\,s^{-1}$)
X	conversion rate
z	coordinate in length of the reactor (m)

Greek letters

α	control activity
β	friction coefficient (s^{-1})
ε	porosity
λ	thermal conductivity ($W\,m^{-2}\,K^{-1}$)
μ	dynamic viscosity (Pa s)
ν_{ij}	stochiometric matrix
ρ	density ($kg\,m^{-3}$)
τ	tortuosity
ω	mass fraction

Superscripts and subscripts

Bound	fictive boundary layer
eff	effective
g	gas phase
i	i'th species
iso	isothermal case
In	reactor inlet
Int	location between Pd–Ag-layer and support
j	j'th reaction
Mem	membrane
Out	reactor outlet
Pd	palladium(Pd)–silver(Ag)-layer
rad	radiation
s	solid phase
Sup	support-layer
Surf	location on surface of Pd–Ag-layer
Shell	shell side of reactor
0	reference conditions

as the partial oxidation, which could lead to higher amounts of carbon monoxide. But due to the fact that they are restricted by the methane concentration, towards the end of the reactor where almost 100% of methane conversion is reached, the WGS reaction is dominant leading to smaller amounts of CO in the exhaust gas.

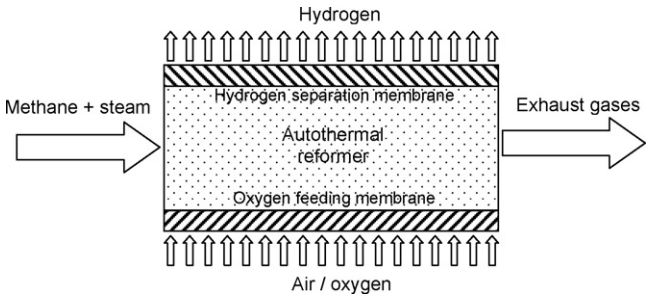

Fig. 1. Autothermal reformer with hydrogen separation and distributed oxygen feed.

A common problem in autothermal reforming concerns the temperature distribution profile in steady-state operation, which is not only severe as illustrated below in Fig. 5 but also detrimental to the system operation owing to unequal time scales of the reactions involved [5,10,11]. The very fast oxidation rate of methane will lead to a temperature peak shortly after the entrance that is disadvantageous in terms of system material strain, especially sealing, membranes, catalysts as well as with respect to reactor performance.

From the work of Tiemersma et al. [5] and Barrio et al. [12] it can be concluded that injecting oxygen at several points over the length of the reactor instead of premixing it with the other gases in the inlet has the ability to reduce this temperature hot-spot. Analogous to the hydrogen removal membrane, a possible and not very cost-intensive realisation method could be an oxygen feeding membrane illustrated in Fig. 1.

With reference to the aforementioned membranes, the main aim of this work is to identify properties and parameters of a targeted design.

Previous optimisation investigations of the membrane design focused in isolation on single aspects only. For example, a lot of research has been done on improving permeability and selectivity of hydrogen separation membranes [13–18] or meliorating the reactor process control [5,12,19]. However, it is possible that upon integration of these aspects into the system the optimization criteria of the components might change.

The aim of this study is to provide an understanding of the membrane reactor as a complex network of interacting phenomena and to identify parameter sensitivities. The hypothesis is that knowing the sensitivities allows the elimination of the systems bottle neck and therefore to concentrate further on efficiency improvement of clearly defined targets. As an outcome of this investigation, the know-how of smart materials design for hydrogen separation and oxygen feed that interact ideally with reaction system subject to operational constraints should be identified.

To simulate the interaction of ATR-reaction system and the hydrogen membrane, a one-dimensional model was used and validated with experimental data as described in Section 2. Further, with regards to the interactions of reaction system and fluid flow, a more detailed state-of-the-art model was used, too for validation as shown in Section 2. The results with the hydrogen membrane experiments are given in the result chapter as well as the description of the oxygen feeding model.

By using the reactor as a spatial control system we integrated the oxygen feeding membrane as a controller to investigate several theoretical approaches like a spatial PID-controller and real membranes of diffusion type and of pressure forced convective type. These results are given in the same chapter.

2. Simulation model

2.1. Fluid flow and reaction model

In this work a one-dimensional model was employed to compute both the process parameters notably temperature and concentrations in addition to the fluid flow parameters namely pressure and velocity in an autothermal reformer. The model is based on a simplified formulation of the conservation equations for mass, momentum, overall energy and species in one dimension while neglecting dispersion effects for a presumed steady-state of operation.

Because of these assumptions the equation set reduces to a system of ordinary differential equations thereby enormously reducing the computational load. The simplification of the equation set was arrived at due to the expected weak influence of the dispersion terms on the interactions between components in the reforming unit and possibility to easily make the reformer model behave like a "spatial control system", that is explained in more detail in Section 3.

In order to ensure that the outcome of the simulation exercise remains comparable to that obtained from solving the entire equation set, in what has established itself as state of the art approach in modelling autothermal reforming [5,19], a comparison is drawn between the results obtained in the developed model and a second one based primarily on the work of Tiemersma et al. [5]. This is done with focus on the membrane flux and the temperature hotspot that are of great interest in this investigation. To distinguish the two models from each other, they are referred to as fast model 1D (FM1D) and the detailed model 1D (DM1D), respectively. The detailed model is described in Appendix B.

As mentioned above, for the FM1D a one-dimensional, pseudo-homogeneous phase formulation of the conservation equations for mass, momentum, over-all energy and species in steady-state operation was applied. The constituting equations are expressed as

$$\frac{\mathrm{d}(\varepsilon\rho_\mathrm{g}u)}{\mathrm{d}z} = \frac{4}{D_\mathrm{R}}\sum_i M_i J_i^\mathrm{Mem} \tag{1a}$$

$$\frac{\mathrm{d}(\varepsilon\rho_\mathrm{g}u^2+\varepsilon p)}{\mathrm{d}z} = -\beta\varepsilon\rho_\mathrm{g}u \tag{1b}$$

$$\frac{\mathrm{d}(\varepsilon\rho_\mathrm{g}uT)}{\mathrm{d}z} = \frac{(1-\varepsilon)\rho_\mathrm{s}}{c_{\mathrm{p,g}}}\sum_j r_j\Delta H_j \tag{1c}$$

$$\frac{\mathrm{d}(\varepsilon\rho_\mathrm{g}u\omega_i)}{\mathrm{d}z} = (1-\varepsilon)\rho_\mathrm{s}M_i\sum_j \nu_{ij}r_j + \frac{4}{D_\mathrm{R}}M_iJ_i^\mathrm{Mem}. \tag{1d}$$

From Eqs. (1a)–(1d), the convective fluxes for the volume-specific properties mass flux, momentum, energy and the weighted mass fluxes for the different species are presented. In the momentum equation, the total momentum which includes the pressure was added to the convective flux. Through this procedure and by neglecting dispersion effects only volumetric sources and no area effects such as additional fluxes or for example pressure forces are included in the momentum equation.

The source term in the mass conservation Eq. (1a) and of course the last term in the species Eq. (1d) depend on the molar fluxes J_i^Mem of every species that permeates through the membranes and can therefore be logically interpreted as area fluxes, however in the 1D-models they can be handled like volumetric sources. This is because the conversion from area-dependent to volume-dependent terms can easily be done by a factor f. For a tubular reactor, f will be given by the relation

$$f = \frac{A}{V} = \frac{\pi D\Delta z}{\pi(D^2/4)\Delta z} = \frac{4}{D_\mathrm{R}}. \tag{2}$$

Typically in 2D- and 3D-models these flux terms appear as boundary conditions.

Owing to the specific interest in only the disappearance of hydrogen and the appearance of oxygen or air in this study, all other membrane fluxes are neglected. This is a reasonable assumption for selective membranes and consequently all the flux rates are set to zero. The details concerning both the hydrogen and the oxygen membranes model are explained in subsequent chapters. In the two cases the flux rates are set to zero at the beginning of the simulations.

Additionally, the pressure loss or convective flux of momentum is determined by the half empirical Ergun-equation given as

$$\beta_\mathrm{P} = 150\frac{(1-\varepsilon)^2}{\varepsilon^3}\frac{\mu_\mathrm{g}}{\rho_\mathrm{g}d_\mathrm{H}^2} + 1.75\frac{1-\varepsilon}{\varepsilon^2}\frac{|u|}{d_\mathrm{H}} \tag{3}$$

with slightly changed coefficients adapted specifically to this problem. The emerging parameter d_H is for this case not a physical but a hydraulic parameter, meaning that the existence of real particle or pore with this diameter is not a prerequisite.

Further, for modelling the reaction system, similar kinetic equations applied successfully in the work of Tiemersma et al. [5] which are based on the experimental study of Numaguchi and Kikuchi [20] concerning the steam-reforming and the water gas shift and on the work of de Smet et al. [21] for the methane combustion are employed.

These models were initially obtained by correcting the experimental results of Trimm and Lam [22] through replacing the Pt/Al_2O_3-catalyst with Ni/Al_2O_3-catalyst, so that a kinetic expression based on Ni was obtained in all the reactions. A short summary of this reaction model is included in the Appendix. According to de Smet et al. [21] the indirect partial oxidation of methane is considered in this model to take place through the methane total oxidation, the steam-reforming and the water-gas-shift on the catalyst surfaces. Due to the work of Tiemersma et al. [5] the intra-particle limitations of heat and mass diffusion was neglected since the catalyst particles are small enough (d_h = 0.5 mm).

Although the equation set ((1a)–(1d)) is reduced to a set of ordinary differential equations, the solution procedure is not trivial. Due to the different time scales of the reaction rates and the deviations in the flow- and pressure-fields, this is a so-called stiff problem. Additionally, has to be taken on the implicit formulation of the pressure in the momentum Eq. (1b). In the employed procedure, decoupling the species Eq. (1d) from the rest was carried out by solving it to determine only the mass fractions but not the total mass load. This makes it necessary to solve the whole equation set although it is overstated in the analytical formulation, because global and component mass balances are of course not independent. This procedure allowed the handling of Eqs. (1a)–(1c) in a different way compared to the Eq. (1d). However, the equation set ((1a)–(1c)) is still a stiff problem due to the total energy conservation Eq. (1c), but the pressure can be corrected after extraction from the conversation variables with the equation set (1d). The remaining problem can then be solved by a common stiff solver like the Rosenbrock formulas [23] that was used in this work.

2.2. H_2-membrane flux model

Because the permeability of the hydrogen through the separation membrane plays a major role in this study, we must explain this model more in detail. The most widely applied membrane materi-

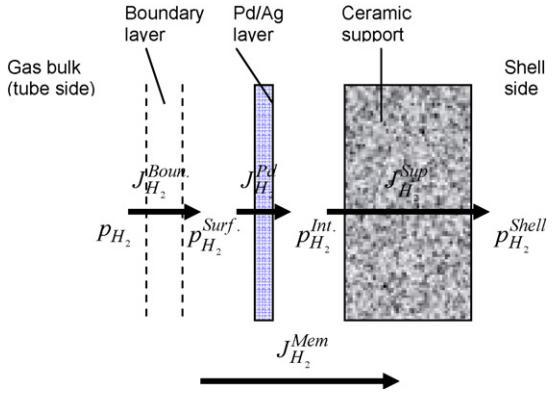

Fig. 2. Schematic representation of three resistance layers describing the hydrogen flux through a separation membrane.

als for the separation of hydrogen gas from a gas mixture are the dense palladium layers and porous zeolite layers, whereby the former secures almost infinite selectivity of hydrogen. The hydrogen flux through both layers depends strongly on their thickness, meaning that in technical applications very thin layers supported with porous materials to enhance the mechanical stability are used. In the proposed model a very thin palladium–silver layer supported on a porous temperature-stable ceramic such as Al_2O_3 forms the optimal separation membrane for hydrogen production at a purity level needed for PEM-fuel cells.

The mass transfer rate through such a composite membrane can be estimated by a model combining the transport mechanisms therefore determining the diffusion rates through the separated layers (Fig. 2) assuming a steady-state operation. This is expressed as

$$J_{H_2}^{Mem} = J_{H_2}^{Boun.} = J_{H_2}^{Pd} = J_{H_2}^{Sup}. \quad (4)$$

In many studies [15,16,18,23] it is shown that at normal operation conditions with common state of the art membranes, the solution–diffusion mechanism which determines the flux in the Pd/Ag-layer is the limiting step and that the flux rate can be described by the Sievert's law

$$J_{H_2}^{Pd} = \frac{Q_{Pd}(T)}{d_{Pd}} \left[\left(p_{H_2}^{Tube}\right)^{0.5} - \left(p_{H_2}^{Shell}\right)^{0.5} \right]. \quad (5)$$

However this is only true for a small range of conditions, especially when the thickness of the Pd–Ag-layer is highly reduced or when the support plays a much stronger role [15,23]. In this work, a more detailed model is applied in order to consider such influences thereby improving the conventional membrane theory.

For describing the molar flux per square meter through the palladium membrane, the more general Richardson's law

$$J_{H_2}^{Pd} = \frac{Q_0^{Pd}}{d_{Pd}} \exp\left(-\frac{E_{act}^{Pd}}{RT}\right) \left[\left(p_{H_2}^{Surf.}\right)^n - \left(p_{H_2}^{Int.}\right)^n \right] \quad (6)$$

was used allowing to vary the order of pressure dependence, too. This can take into consideration defects in the palladium matrix and surface effects measured in experiments [15,24].

For the determination of the gases diffusion through porous media like the open porous support ceramic, often the dusty gas model [24] is used. The dusty gas model is actually a combination of the Stefan–Maxwell-equation, Knudson-diffusion and viscous flow. Assuming that only hydrogen located in the support exists, the model reduces to a sum of the two last mentioned mechanisms and can be expressed as

$$J_{H_2}^{Sup} = \frac{8}{3}\sqrt{\frac{8}{\pi RTM_{H_2}}} K_0 \frac{p_{H_2}^{Int.} - p_{H_2}^{Shell}}{d_{Sup}} + \frac{B_0}{\mu_{H_2} RT} \frac{\left(p_{H_2}^{Int.}\right)^2 - \left(p_{H_2}^{Shell}\right)^2}{d_{Sup}}. \quad (7)$$

The use of a 1D-model to compute the reactions and the flow in the reformer that cannot consider the dispersion of mass or the mass transport to the membrane directly, necessitates the introduction of a third layer referred to in this work as a boundary layer which contributes to the flux resistance. Hou et al. [15] showed that the flux through such a layer can approximately be evaluated by a Maxwell–Stefan formulation. Assuming that the fluxes of the other species towards the membrane are relatively small in the boundary layer compared with hydrogen, the hydrogen flux can be evaluated using the relation

$$J_{H_2}^{Boun.} = \frac{(\varepsilon/\tau)}{\sum_{i,i\neq H_2} p_i / D_{i,H_2}} \frac{p_{H_2} - p_{H_2}^{Surf.}}{d_{Boun.}}. \quad (8)$$

In Eqs. (6)–(8) parameters for the structure of the support (K_0, B_0), the structure of the reformer (ε/τ) and the behaviour of the Pd/Ag-layer (Q_0, Ea_{Pd}, n) which have to be determined from experiments are present. In this work parameter results presented in Yang et al. [18], obtained from experiments with Al_2O_3 – supported Pd–Ag – membranes under certain conditions were applied. The results of this validation are given in the next chapter.

2.3. Validation

2.3.1. H_2-separation membrane model

Owing to a great interest in hydrogen purification technologies, a lot of research data can be found concerning hydrogen permeation through Pd–Ag-membranes with porous ceramic support [15,16,18,24] that enables easy verification of the proposed membrane model.

In all these investigations, different experimental conditions, membrane supports and Pd–Ag-coating principles were applied. Nonetheless, because only the behaviour of the model of one type of membrane under different conditions in the autothermal reformer is of interest in this study, focus was put on data from a single experimental set-up. From an initial comparison of the reported results, it was found that the work of Yang et al. [18] was closest to the constraints in autothermal reforming and enough data was available for the verification of the proposed model according to the outlined set of research aspects.

Noting that the behaviour of one type of separation membrane or one set of parameters at different temperatures and pressures is very important, Yang et al. [18] measured the hydrogen flux at different temperatures and differential pressures of 1, 4 and 8 bar where hydrogen was present in pure form on both sides of the membrane. In this work, one set of parameters for the proposed model that best fits all measurement points was determined and presented in Table 1.

Following a direct comparison with the results from Yang et al. as presented in Fig. 3, it can be concluded that the proposed model describes the temperature and pressure dependence quite well, more precise at higher temperatures compared to lower temperatures. Furthermore, due to the relatively small temperature differences that are between 400 and 600 °C it presents no disadvantage.

The parameters we found, are mostly in the region of values given in the literature [5,15,24]. The pre-exponential factor Q_0 for the Pd–Ag-layer, what describes the hydrogen diffusivity and the hydrogen solubility in the alloy, was found at

Table 1
Parameter sets for the membrane model verification. The first column represents the parameters for the validation case with pure hydrogen permeating through the membrane. The second column describes the validation case, where a gas mixture of 70.2% H_2, 13.5% CH_4, 14.3% CO, 2% CO_2 is located on one side of the membrane and hydrogen is selectively permeating through the membrane

	H_2/H_2	H_2/gas mixture
ε/τ	–	17.676
Q_0	13.435×10^{-9} mol m^{-1} s^{-1} Pa^{-n}	7.162×10^{-9} mol m^{-1} s^{-1} Pa^{-n}
Ea_{Pd}	5.488 kJ mol^{-1}	13.553 kJ mol^{-1}
K_0	3.188×10^{-10} m	3.188×10^{-10} m
B_0	6.835×10^{-15} m^2	6.835×10^{-15} m^2
n	0.588	0.735

13.435×10^{-9} mol m^{-1} s^{-1} Pa^{-n}. The activation energy Ea_{Pd} for the Arrhenius type permeability was 5.488 kJ mol^{-1} K^{-1} and we found a pressure dependence of the order $n = 0.588$. This order is higher than the proposed order of 0.5 from the Sievert's law which would be the case for a pure diffusive flux through this layer. Probably due to the enhanced surface processes at thinner layers which are of order $n = 1$ [15], its order must be in-between these limits. The parameters for the support, the Knudson coefficient K_0 and the Permeability B_0 were found at 3.188×10^{-10} m and 6.835×10^{-15} m^2, respectively are probably too high [24], but due to the fact that the influence of the support enhances with thinner Pd–Ag-layers this presents no disadvantage to our simulations. This is therefore dedicated to the worst case meaning a strong flow resistance in the support.

Equally important in this investigation is the behaviour of the membrane when subjected not only to hydrogen on one side but a mixture of gases, as is typical under normal operation conditions in separation membranes. For this purpose, a methane membrane reformer was employed and the gas mixture consisted mainly of hydrogen, methane, carbon dioxide and carbon monoxide. Yang et al. measured the hydrogen flux through the membrane at different temperatures and differential pressures staring with a gas mixture with composition 70.2% H_2, 13.5% CH_4, 14.3% CO, and 2% CO_2 on the tube side.

Again the best parameter set for all measurement points was determined for the mixture while we left the parameters for the support constant assuming that only hydrogen is permeating

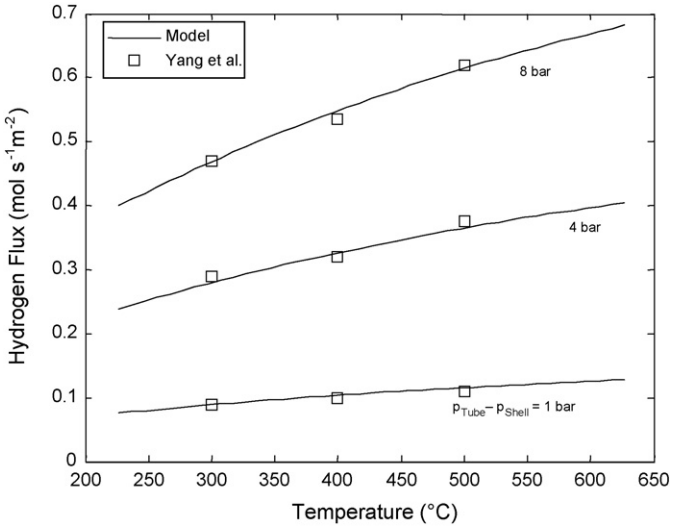

Fig. 3. Hydrogen flux through a 1.5 mm thick Al_2O_3-support covered with a 20 μm thick Pd–Ag-layer at several differential total pressures and temperatures—comparison of FM1D-model results with experimental data taken from Yang et al. [18].

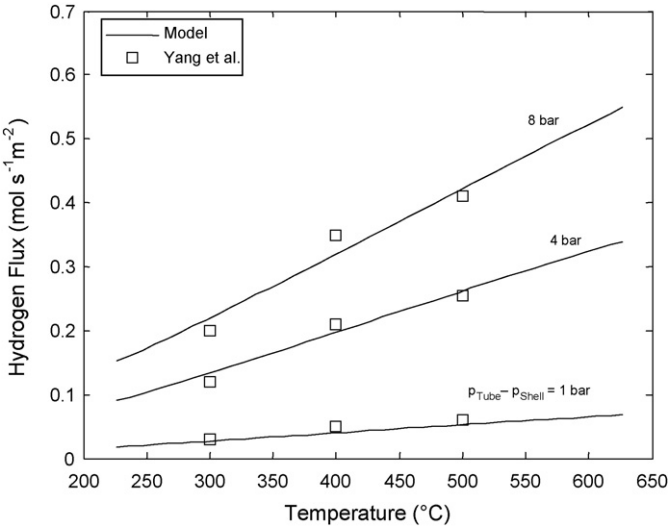

Fig. 4. Hydrogen flux through a 1.5 mm thick Al_2O_3-support with a 20 μm thick Pd–Ag-layer and through a boundary layer with mixed gases (70.2% H_2, 13.5% CH_4, 14.3% CO, 2% CO_2) on the tube side at several differential total pressures and temperatures.

through the Pd–Ag-layer. The results presented in Fig. 4 shows that the proposed model describes the dependences on temperature and pressure very well, however a quite different parameter set (Table 1) must be used. Especially the carbon monoxide is dedicated to influence the permeability of the membrane since it contaminates the Pd–Ag-layer. Thereby the pre-exponential factor Q_0 sinks to 7.162×10^{-9} mol m^{-1} s^{-1} Pa^{-n} and the activation energy Ea_{Pd} rises up to 13.553 kJ mol^{-1} what means that more energy is necessary to permeate hydrogen through the membrane. Also, the order of pressure dependence was increased to an order of $n = 0.735$, but this is also in the line with values given in the literature [5]. In this case an additional flow resistance must be considered which is represented in the model by the boundary layer (Eq. (8)). The only parameter in this layer was the porosity tortuosity ratio and its value was found to be 17.676 what is probably too high comparing to given literature data [24].

Moreover, because this represents the normal operation conditions of the separation membrane the obtained parameter set were used in all subsequent simulations.

2.3.2. Validation of the FM1D

In this model, the thermal and mass dispersion in the FM1D are neglected and a steady-state condition for our simulations is assumed. With respect to these simplifications, a proof of the correctness of the model has to be performed, further as already mentioned elsewhere above, this was carried out by direct comparison with another more detailed model (DM1D) according to the research issues.

The model, described in detail in Appendix B, considers dispersion effects and reaches the steady-state after several unsteady iterations referred to as quasi-steady-state. The DM1D has already been used and verified in many research work [5–7,19], it has established itself as a state-of-the-art model for autothermal reforming, consequently the suitability of the proposed model can be confirmed through a direct comparison where deviations can be quantified.

As a representative of the many simulations carried out, the adiabatic case without any membrane (Table 2) was selected and used as a reference case for every other simulation. Comparison of the temperature profiles resulting from the simulations done with

Table 2
Parameter set and boundary values for the adiabatic base case

Parameter	Value
$\dot{m}_{CH_4}$	1.42×10^{-5} kg s^{-1}
T_{In}	600 °C
p_{Out}	1.013 bar
$(O_2/CH_4)_{In}$	0.379
$(H_2O/CH_4)_{In}$	1.621
ε	0.45
L	0.1 m
D	0.02 m
Δz[a]	5×10^{-4} m

[a] Spatial resolution in the length of the reactor only for DM1D.

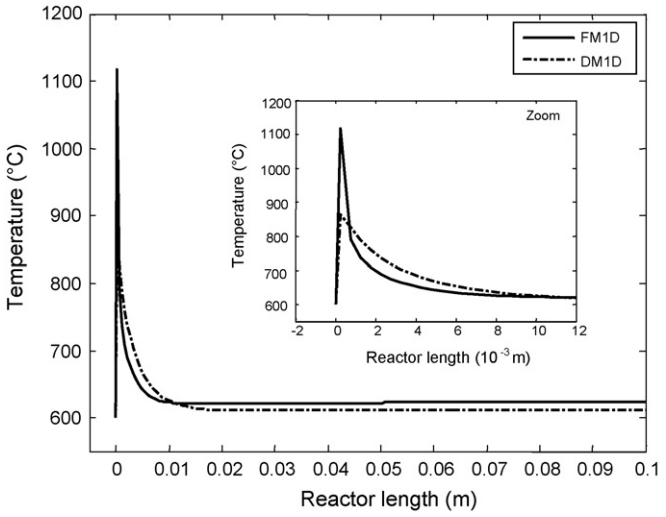

Fig. 5. Comparing the temperature profiles of the FM1D and the DM1D-model for the adiabatic base case.

FM1D and DM1D is shown in Fig. 5. The obtained profiles serve as indicators of the suitability of the proposed model. From the results shown in Fig. 5, it can be seen that the temperature peak in the DM1D is located in a region between the inlet and 0.02 m with a maximum temperature of 865 °C compared with the FM1D-profile which is in the region up to 0.012 m with a maximum temperature of 1117 °C. This could be due to the influence of the thermal dispersion. Further, a lower equilibrium temperature for the DM1D of about 615 °C is observed compared with 623 °C for FM1D. This can be attributed to the wider peak profile, because in the region where the temperature is high, the steam-reforming is much stronger than the water-gas-shift. This implies that in the entrance region, the DM1D-model predicts more energy usage for this reaction than in the FMID, this causes the establishment of equilibrium further away from the entrance at a lower energy level.

Nonetheless, both models show great similarities in predicting the main behaviours especially the appearance of the temperature peak and the equilibrium temperature is with a deviation of only 1.3%. This means that the proposed model describes the ATR-reactor very well within very small error limits.

3. Simulation results

3.1. Hydrogen separation membrane

As already mentioned in Section 1, the research of membranes for hydrogen gas separation has reached a high level in contrast to the use of these membranes directly in reformer stages that are still in the early research stages. The targeted advances are of course

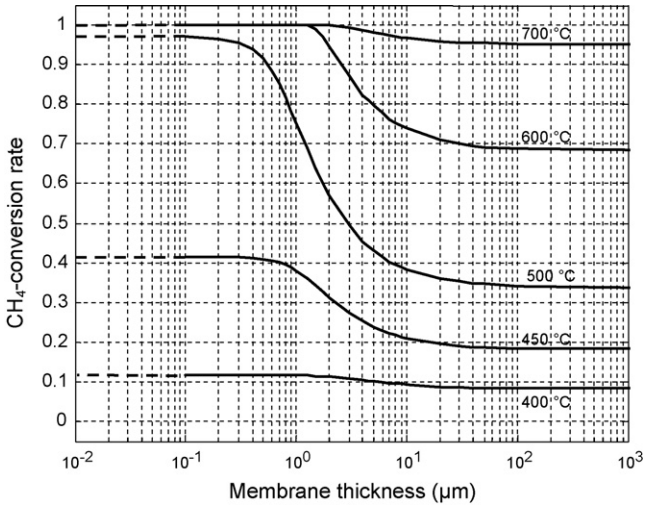

Fig. 6. Conversion rates of CH_4 at different operating temperatures in the isothermal depending on membrane thickness.

the possibility of producing hydrogen at high purities and a better utilization of catalyst in the reformer.

However, most studies are concerned with maximizing the permeability as well as the selectivity, referred to here as permselectivity. The results from such investigations typically suggest a very thin Pd–Ag-layer supported with an open-porous structure to attain very high mechanical stabilities.

In technical applications there are often different constraints and in the case of hydrogen separation membranes an optimum between thermal, mechanical and operational properties of the membrane has to be determined. In this part of the investigation, hints for designing optimal membranes instead of membranes that are drilled for optimizing only one property was carried out.

As a first step, the thickness of Pd–Ag-layer that is really necessary for the use in an ATR-reactor was found out. This is because through minimizing the thickness of Pd–Ag-layer a better permeability will be achieved but at the expense of the mechanical strength as well as the thermal stability or the resistance to thermal shocks.

For a deeper understanding of the relevant issue, the proposed model was reduced to an isothermal operation, which should be the ideal case for producing hydrogen as described in detail in Section 3.2. This made it possible to simulate the equilibrium state at different temperatures easily.

Several simulations were run at specified by varying the thickness of the Pd–Ag-layer of the separation membrane. The operational pressure in the reactor outlet was 1 bar and the partial pressure of hydrogen on the shell side we set to zero in order to get maximum pressure differences.

In Fig. 6, a plot of the conversion rates of CH_4 in an ATR-Reactor at different operational temperatures T = 400, 450, 500, 600 and 700 °C was performed. The membrane thickness in the ordination axis is presented in a logarithmic scale to permit clearer view of the effects.

From the plot, it can be deduced that for temperatures below 400 °C and above 700 °C the variation of membrane thickness has only marginal influence on the performance. This is due to the optimal temperature region of the reforming reaction, which is about 550 °C. Even more significant, is that in between these two limiting temperatures the region of transition is almost the same for all calculated temperatures ranging from 0.2 to 30 μm. Furthermore, from Fig. 6 it can be seen that the thickness of the Pd–Ag-layer is for some region of temperature the limiting step. Reducing the thick-

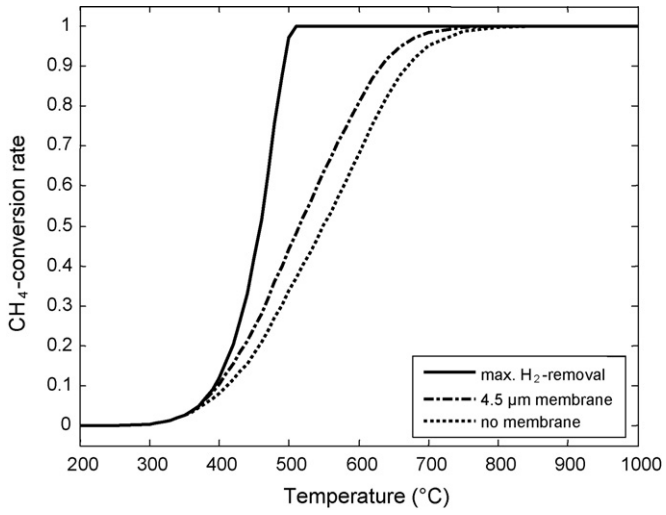

Fig. 7. Conversion rates of CH_4 for different membrane types at different operating temperatures.

ness of this layer means that this barrier decreases until it is not longer the main limiting step.

It therefore means that removing the systems bottle neck with respect to the membrane involves the use membranes with thicknesses below a value of about 400 nm. If so, the process can be considered as unconstrained by hydrogen diffusion through the membrane and solely depending on reaction rates, diffusion from bulk gas to catalyst as already considered in the used reaction model [21] and the removal of hydrogen, which means the three diffusion barriers of the separation membrane mentioned in the former chapter.

Even though a wide range of Ag–Pd-layer thickness (from 10 nm to 1 mm) was considered, the model was only validated for a 20 μm thick Pd–Ag-layer. For much thinner layers, such as below 100 nm, it is well-known, that the solution–diffusion model cannot describe the hydrogen flux through this layer accordingly due to surface processes and other influences. Also with state of the art technologies used for producing such membranes the pore sizes of the support decrease with decreasing thickness of the Ag–Pd-layer. Thereby, the influence of the support is increasing. For these reasons dashed lines were used in Fig. 6 for layer thickness below 100 nm to show that in this region the results are possibly not valid.

Fig. 7 shows the same results as in Fig. 6 but in the conversion-temperature plane. In this case the region of influence of the membrane can be seen better. This plot presents the conversion rates of CH_4 for specified membrane thickness as a function of temperature. In the plot, the dotted curve represents the case when no membrane is used, what represents one limit in the range of thickness. In the region of interest the conversion rate represented by this curve tends to unity.

Similarly, in the case represented by the solid line which is a theoretical super thin-membrane or membrane thickness with thickness tending to zero ($d_{pd} \to 0$). In real membranes the characteristic curve of the conversion-rate against the temperature-should fall in between the two limits.

From Fig. 7, the dash-dotted line corresponds to a modern separation membrane from current research [15] representing state of the art for membrane thicknesses. From this investigation, it was found out that a difference between the state of art membrane thickness and the limiting thickness at 400 nm exists as is evident from the gap between the two curves representing extreme cases in Fig. 7. This points out the necessity for further work in this area to achieve the limiting value of membrane thickness. However,

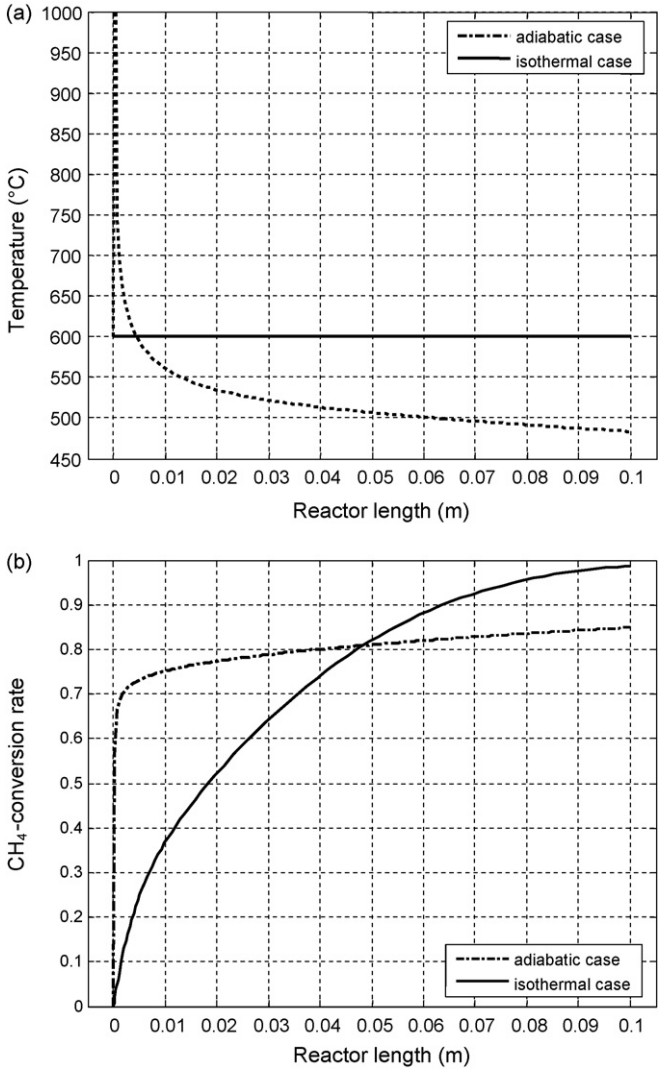

Fig. 8. (a) Temperature $T(z)$ and (b) CH_4-conversion $X_{CH_4}(z)$ profiles in a membrane reactor with maximum hydrogen removal within the isothermal and adiabatic case.

it should be noted that this only represents a limit value and that it is necessary to optimize membranes according to their applications.

3.2. Oxygen control

As mentioned above the isothermal operation of the ATR can be considered as the ideal case in contrary to the adiabatic case that represents the other extreme mode of operation. In Fig. 8a the temperature profiles for the two cases are shown over the length of an ATR-reactor with maximum hydrogen separation to make a maximum conversion of CH_4 possible. For the adiabatic case, there is a temperature peak directly at the entrance of the reactor. This is a major problem with the autothermal reforming also identified in [10]) owing to a strong thermal stress which can lead to destruction of catalyst or the separation membrane. Another aspect is addressed in Fig. 8b showing the conversion profile of CH_4. In the adiabatic case almost all the conversion is done near the entrance corresponding to the temperature peak. The reforming reaction after this region with the main conversion by partial oxidation is reduced because there is only few CH_4 left for producing hydrogen and the ongoing increasing caused by the hydrogen removal is quite

small. This means that the greater part of the reactor has no use for producing hydrogen.

In comparison to the adiabatic steam-reforming much better profiles are obtained in the isothermal case, without peak temperatures, but evident from the results presented in Fig. 8b shows a much better distributed reaction over the entire reactor leading to a better utilization ratio of the catalyst.

By using a membrane that theoretically removes all hydrogen, the theoretic maximum of CH_4-conversion rate can be reached even after a short reactor length $L = 0.1$ m. In the adiabatic case where the increase is relatively smaller, there is need for a longer reactor to achieve the equal conversion rate. The reason for this can be found in the temperature profile of the adiabatic case, where the temperature decreases very strong along the reactor with respect to the ongoing reforming reaction without additional energy source like the partial oxidation.

With knowledge of the two cases representing extreme limits of the ATR-process, the goal should be the attainment or approaching of the isothermal case. As a possible solution Tiemersma et al. [5] proposed and came to the result by simulation, that a linear feeding of oxygen over the length of the reactor also leads to a poor temperature distribution, an exponential feeding might be possible however, it was not investigated. Similarly a staggered oxygen feeding will make the design of small scale reactors too complex and even the temperature peaks cannot be avoided.

A further approach is given in the work of Barrio et al. [12] who split the feed of oxygen and steam and optimized the locations and amounts of injecting. They came to the conclusion that this can damp down the temperature profile but still has the same disadvantages as found in the work of Tiemersma et al.

Outgoing from this and considering the interactions between the reactions and the oxygen feed, it could be a good idea to have a "spatial control system" for oxygen feed to the reactor. This means that we have a continuous (or almost continuous) feeding with different fluxes at different positions depending on the reactor performance. This could be realized by means of an oxygen separation membrane due to the difference between the partial pressures on shell and tube side allowing to spatially controlling the flux through this membrane. Alternatively, a membrane with distributed pore sizes or membrane thickness would allow a spatial control.

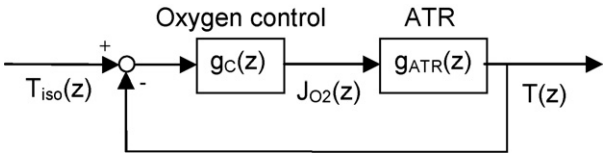

Fig. 9. Spatial control system for the reactor depending on the temperature $T(z)$ to the location z in length of the reactor.

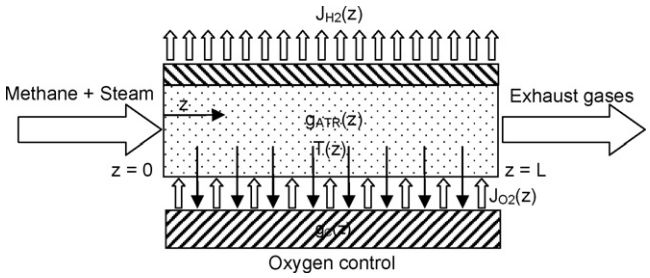

Fig. 10. Visualisation of the spatial control system in the membrane reactor.

To define targets for developing such a membrane, the identification of necessary flux control conditions for approaching the isothermal case was carried out. Further, the FM1D-model as representation of the reactor system was used and implemented into Matlab/Simulink, forming a spatial control system for oxygen feeding using space coordinate z instead of time as variable as illustrated in Fig. 9. Because the isothermal case was considered as an ideal one, the temperature will be used in the reactor as feed-back variable and the oxygen flux used for controlling the reactor behaviour (Fig. 10).

The used controller are listed in Table 3 and will be described with the results in detail. To make the proposed O_2-flux which is referred to the reactor surface more comparable to the fluxes in the inlet which are not, we introduce a parameter $\alpha(z)$ and a

Table 3
A list of the used controller and the estimation of the parameter $\alpha(z)$, respectively

Controller	Estimation of $\alpha(z)$	Description
Relay	$\alpha(z) = \begin{cases} 1 \\ 0 \end{cases}$ for $\begin{matrix} T(z) < T_{\min} \\ T(z) > T_{\max} \end{matrix}$	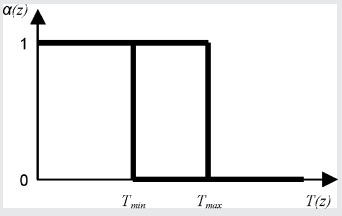
Saturation	$\alpha(z) = \begin{cases} 1 \\ \dfrac{T(z) - T_{\max}}{T_{\min} - T_{\max}} \\ 0 \end{cases}$ for $\begin{matrix} T(z) < T_{\min} \\ T_{\min} \le T(z) \le T_{\max} \\ T(z) > T_{\max} \end{matrix}$	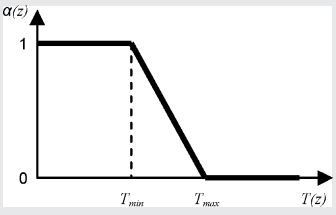
PD	$\alpha(z) = K_P(T_{iso} - T(z)) + K_D \frac{d}{dz}(T_{iso} - T(z))$	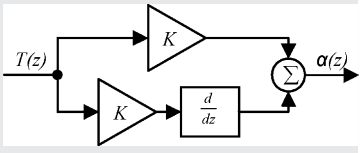

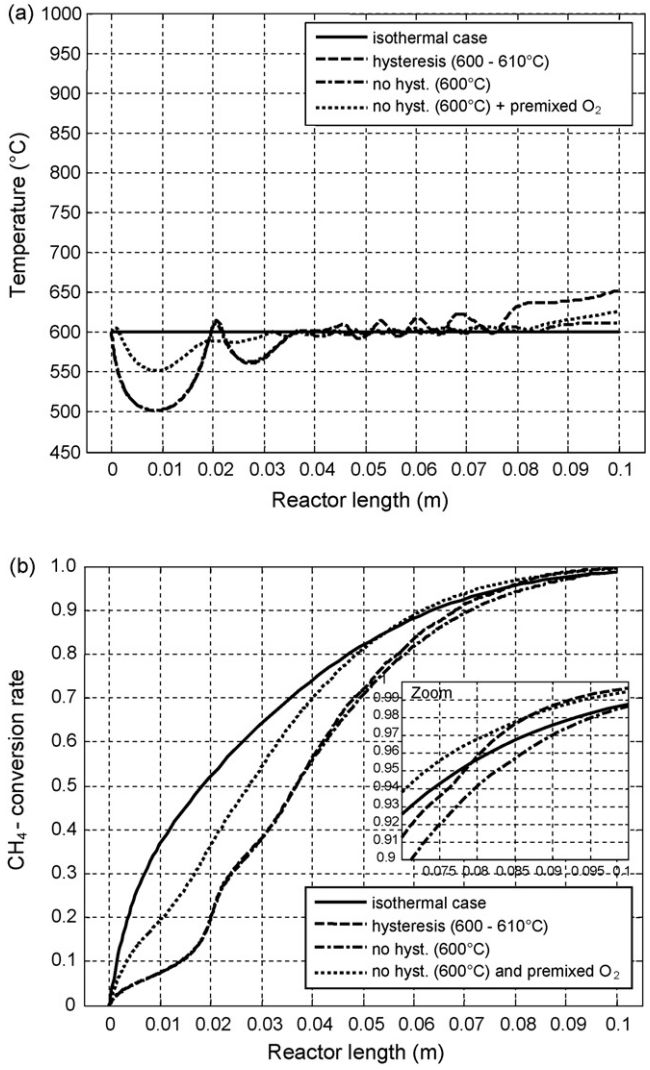

Fig. 11. Temperature (a) and CH4-conversion (b) profiles for the oxygen feeding with relay controls with and without hysteresis compared to the isothermal case.

$(O_2/CH_4)_{\alpha=1}$—ratio. These are defined by the equation

$$J_{O_2}(z) = \frac{(O_2/CH_2)_{\alpha=1}\alpha(z)}{\Delta A_{O_2}(z)}\dot{n}_{CH_4} \quad (9)$$

for the molar flux of oxygen per square meter at the position z of the length of the reactor. The given flux ratio $(O_2/CH_4)_{\alpha=1}$ is the ratio of the summerized oxygen flux over the reactor length referred to the methane flux at the inlet when $\alpha(z) = 1$ for all positions z. The parameter $\alpha(z)$ is the control activity of the used controller and its estimation is given in Table 3, respectively.

3.2.1. Relay control

In the simulation a control with a relay characteristic was used, which is essentially a switch between the states oxygen flux-on and oxygen flux-off (Table 3). The decision for switching is done with a slight hysteresis that depends on two temperatures T_{min} and T_{max}. When the temperature in the reactor is over T_{max}, the flux switches off and when it is under T_{min} it switches on, so that oxygen is fed to the reactor.

The ratio of oxygen flux referred to methane flux (Eq. (9)) was set to $(O_2/CH_4)_{\alpha=1} = 0.568$ for every pair of minimum and maximum temperatures. In Fig. 11 two cases or sets of these temperatures can be seen, one with a hysteresis region between 600 and 610 °C and another without hysteresis switching to on and off at 600 °C. To compare these concepts with the ideal isothermal case its temperature profile and conversion profile for an operating temperature of 600 °C are also presented in the diagrams. For a better understanding on how the controller reacts on the temperature, a relation of the control activity and the temperature in the reactor for the case with hysteresis is exemplarily presented in Fig. 12. From here the points of on and off switching of oxygen is clearly visible.

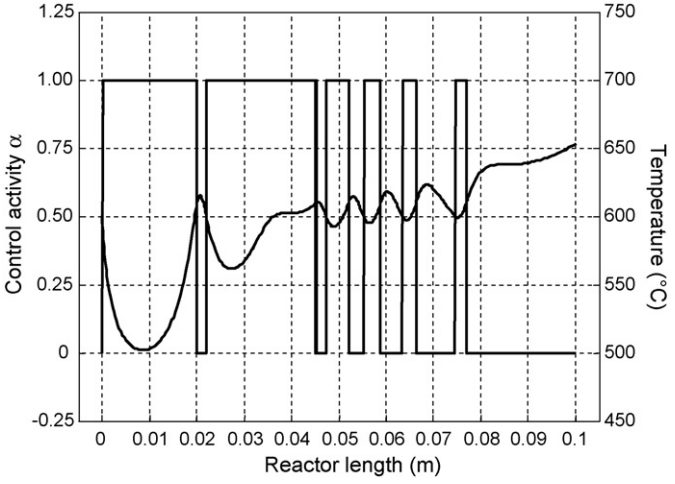

Fig. 12. The Control activity profile compared to the according temperature profile of the simulation case with hysteresis.

In Fig. 11a, the temperature profiles in the reactor over the length of the reactor can be observed for the case with and without hysteresis. Comparing these two profiles, it is obvious, that the maximum temperature difference in the case with hysteresis is relatively high in the range $T = 500$–650 °C compared with that without hysteresis in the range $T = 500$–607 °C.

Furthermore, in both cases the differences are much better than under adiabatic conditions, but in one third of the leading section of the reactor, the temperature falls far under the isothermal line due to the small amount of oxygen at the entrance region.

This could be due to the fact that the maximum flux ratio of $(O_2/CH_4)_{\alpha=1} = 0.568$ is too small for this region. A look at the conversion rate profile it is seen that for both cases at the reactor outlet the controlled processes are very closely to the ideal profile. In the zoom of Fig. 11b the differences between these profiles is seen more clearly. At a reactor length of about 0.08 m the curve representing the case with hysteresis is increasing faster due to the increasing temperature in this region. However, although this conversion rate of CH_4 is higher, the ideal case we have in mind is still the isothermal. A high conversion rate can of course also be reached by just oxidizing all the methane.

To meliorate the temperature falling in the entrance region, premixing of a small amount of oxygen to the inlet gases $((O_2/CH_4)_{In} = 0.06)$ and controlled the reactor without hysteresis and $(O_2/CH_4)_{\alpha=1} = 0.568$ was performed. The temperature and conversion rate profiles according to this are presented in Fig. 11a and b with the dotted line from which we can observe a much better behaviour for both in comparison with the other cases. The conversion profile representing this case is even in the whole reactor length very close to the isothermal case what means that the utilization ratio of the catalyst is very good over-all the length of the reactor.

Another concept to raise the temperature in the first third of the reactor but approaches the isothermal case more precisely, is the use of a saturation control what will be described next.

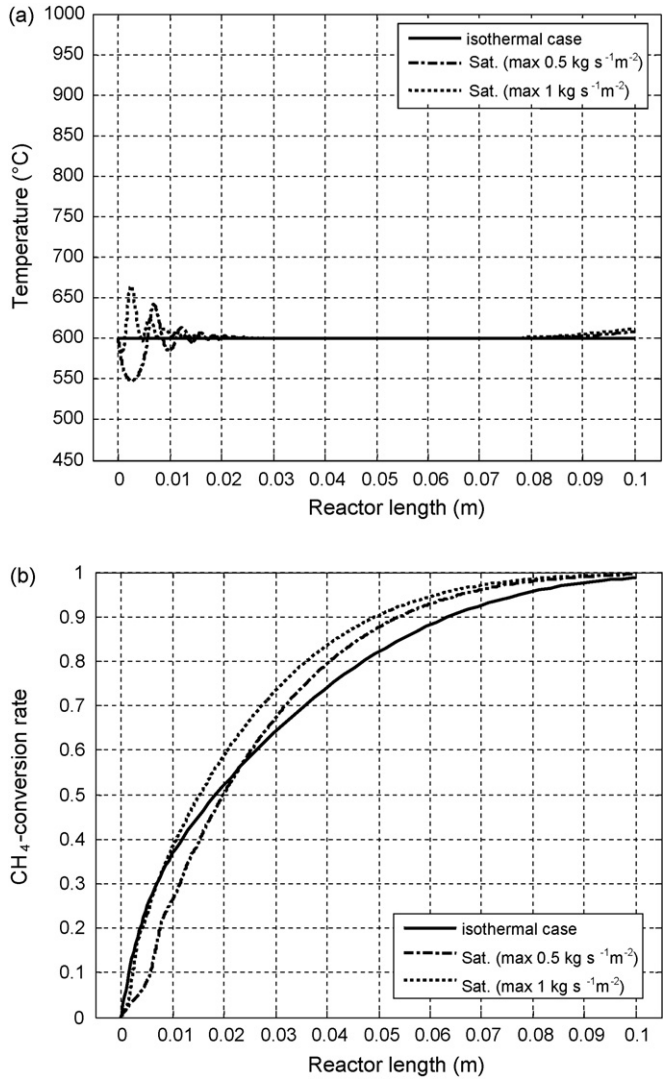

Fig. 13. Temperature (a) and CH_4-conversion (b) profiles for the oxygen feeding with saturation control at different fluxes compared to the isothermal case.

3.2.2. Saturation control and PD

In this simulation the saturation control or more precisely a PD-controller was used to approach the isothermal case. The saturation control (Table 3) has a similar characteristic as the relay control with hysteresis. However it has a switching region inside it in contrast to only an on–off-possibility which intern has a linear characteristic similar to a proportional (*P*) controller.

In fact, this control has a linear dependence on the reactor temperature with an upper temperature limit for maximum flux and a lower temperature limit for zero flux. In the simulation the temperature limits were set to 599 and 601 °C. This is very close to the isothermal temperature of 600 °C to achieve small temperature gradients but not too close for moderate switching times.

In Fig. 13 the temperature and CH_4-conversion rate profiles for two different flux ratios $(O_2/CH_4)_{\alpha=1}$ (3.549 and 7.098) represented by the dash-dotted and the dotted lines, respectively, are shown and compared again to the isothermal case. For the case with the low maximum oxygen flux the temperature behaves similar to the temperature with the relay control, shortly after the inlet the temperature falls due to the small amount of oxygen, but this time only to 550 °C. After this a slight oscillation starts and the isothermal temperature is reached after 0.023 m. The dotted line, representing the case with high maximum flow, sinks only about 10 °C, but leads after this to a new temperature peak reaching 665 °C and after some oscillations 600 °C is reached at about 0.019 m. For both cases at the outlet of the reactor the temperature is again rising what can be explained with a look at the conversion rate profiles. Comparing them with the isothermal profile, the high flux case starts in a very similar way with it and the low flux case has in the entrance region a lower conversion rate due to the lower combustion of methane in this area. But after some length, both profiles cross the isothermal profiles and have a higher conversion rate until the end of the reactor where they meet again the isothermal profile. That means that the steam-reforming of methane is mostly done after 0.08 m and after this the exothermic water-gas shift reaction predominates. For reactor behaviour, this should be no problem and if the temperature increase is not too high, it can be advantageous because of reducing carbon monoxide in the exhaust gases. Therefore, the saturation control might be a good solution for influencing the reactor behaviour and hence give decisively hints for designing real oxygen controller.

Nonetheless, to exhaust all possibilities of spatial controlling, a common controller with PD-characteristic (Table 3) which is possibly the most abstract oxygen control of all mentioned in this work with regards to real possibilities to control the oxygen flux over the length of the reactor. In this concept the possibility to remove oxygen from the reactor is also considered, meaning that it should be possible to reach the ideal profiles with a PD-controller more precisely. Of course, this is not realistic but the knowledge obtained from the best oxygen flux characteristic according to such a controller can enormously be useful in designing realistic concepts.

The layout of the PD-controller was not easy due to the complicated reaction system with ignition of methane combustion and hydrogen removal, but from the behaviour of the reactor it could be assumed that the control system is of low order with high influence of dead time processes. Assuming this and from simulation testing it was found out, that a *P*-characteristic with an amplification of $K_P = 0.5$ and $(O_2/CH_4)_{\alpha=1} = 0.568$ leads to quite good temperature profiles but with sharp oscillations as indicated in Fig. 14.

Adding a small differential (D) part with $K_D = 0.001$ to the controller eliminates these oscillations and due to the low order of the system an additional integral (I) part is not necessary.

Comparing only the temperature profiles in Fig. 14a of these controllers with the relay or saturation controllers it is obvious, that this concept fits the isothermal case best, as was expected. The maximum temperature differences for the P-controller were 23 °C and for the PD-controller even just 2 °C. We found only marginal deviations in the conversion rate profiles from the isothermal case. Also depicted in Fig. 14b are the oxygen flux profiles according to the P and the PD-controllers. The flux supplied from the *P*-controller shows many oscillations and is therefore quite unsuitable as a basis for realistic concepts. The PD-controlled flux, represented by the thick dashed line, does not show such oscillations and seems to be the mean value of the *P*-controlled flux control. With regards to a realistic oxygen control this flux can be divided into two parts. First, there is a high flux in the entrance region, what can be achieved with premixing 10% of the oxygen to the inlet gases. The second part can be described by an exponential function (7) and is therefore conveniently appropriate for designing an oxygen control membrane. Consequently we use this information to determine the permeability function of a real membrane.

3.2.3. Real membranes

From the simulation results of theoretical controllers, focus was put on realistic possibilities to control the reactor behaviour and use the information from the theoretical concepts for designing purposes.

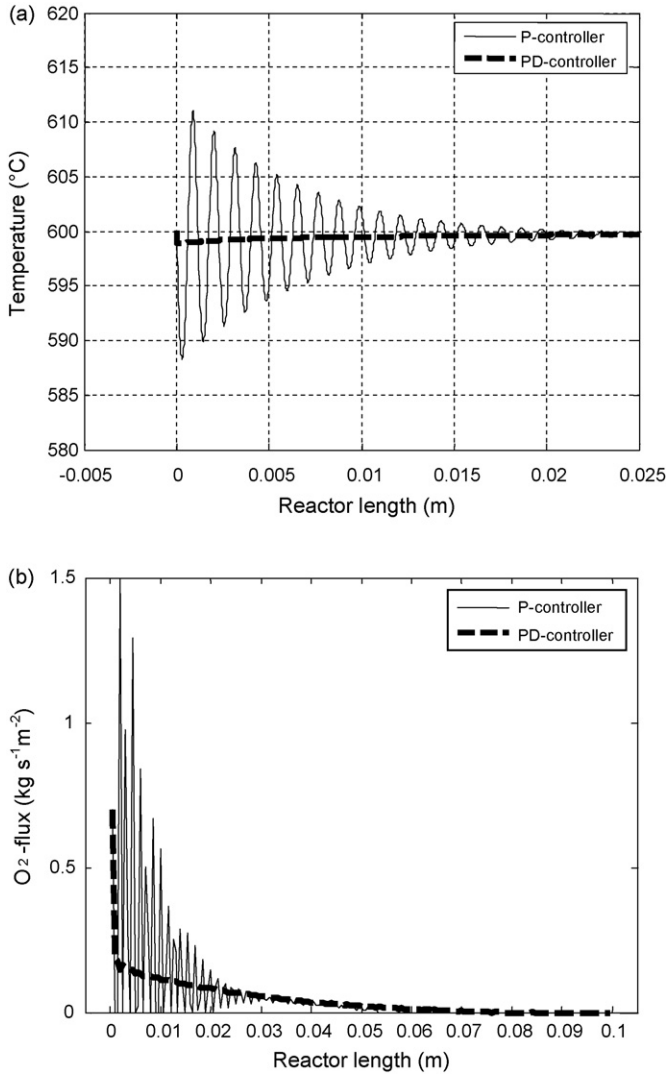

Fig. 14. (a) Temperature profiles for the oxygen feeding with P- and PD-controller and (b) oxygen flux distribution in length of the reactor supplied by the controllers.

When oxygen feeding is used as a control strategy, three possibilities exists notably, oxygen injection systems, diffusion membranes and open porous membranes. Because injection systems are very cost-intensive and will make the reactor much bigger [5,12] and diffusion membranes might not have enough oxygen permeability [9] for the use in an ATR-reactor special attention was paid on open porous membranes that are perhaps the easiest and cheapest way for realisation of an oxygen control concept.

The simplest of these membranes is an open porous structure from ceramics or metal with constant permeability and so with constant pore-sizes, porosity and thickness. Such a membrane can easily be integrated in a reactor and oxygen or air can be fed simply by a small pressure difference between the tube and the shell side of this membrane.

Nevertheless, because it is known that more oxygen is needed in the entrance region than in the rest of the length as is evident from the relay and saturation controls systems, a membrane with a linear decreasing permeability, perhaps due to a linear increasing of the membrane thickness over the length of the reactor could lead to better results.

Applying the simulation results from the PD-controller, it is apparent that the oxygen flux distribution and therefore membrane

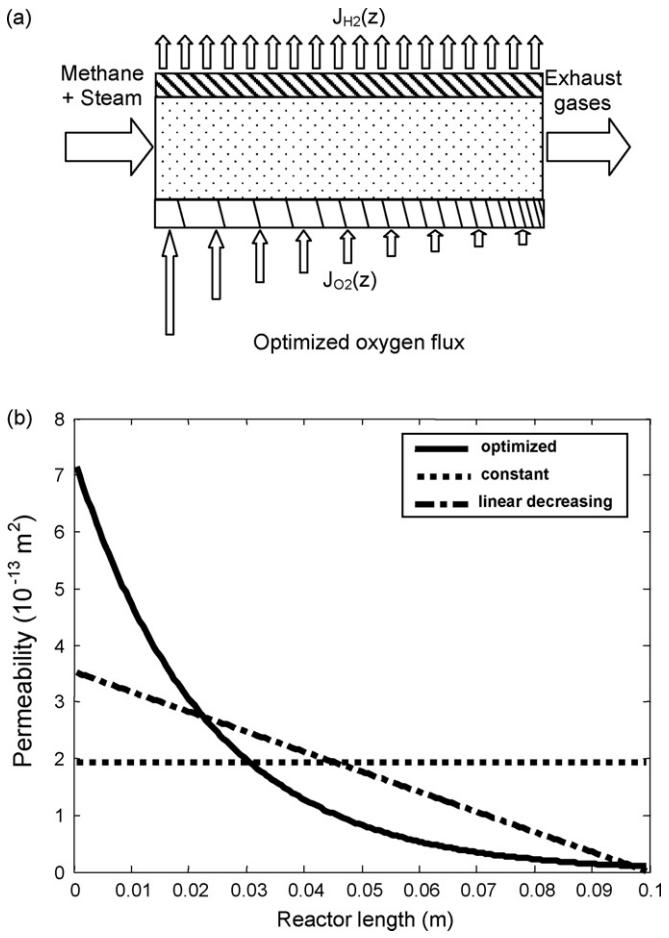

Fig. 15. Oxygen flux profiles through membranes of following properties: constant permeability, linear decreasing permeability and by a PD-controller optimized permeability.

permeability distribution offers the best control strategy for the reactor. In this case the oxygen flux profile from the simulation with the PD-controller led to the best results, shown in Fig. 14b.

As mentioned before, the second part of this flux can be described by an exponential function,

$$J_{O_2}(z) = Ce^{mz} \tag{10}$$

for what we found the best fit with $C = 0.1905\,\mathrm{kg\,s^{-1}\,m^{-2}}$ and $m = -43.5677\,\mathrm{m^{-1}}$. Because real permeation membranes are normally characterized for that purpose with the permeability, the flux profile can be transferred by the Darcy law

$$K_{\mathrm{Mem}}(z) = \frac{\mu_{O_2} d_{O_2,\mathrm{Mem}}}{(p_{\mathrm{Shell}} - p_{\mathrm{Tube}})\rho_{O_2}} J_{O_2}(z). \tag{11}$$

Fig. 15 depicts this optimized profile for a 2 mm thick membrane with a differential pressure of 0.1 bar as well as for membranes with constant and linear decreasing permeabilities leading to equivalent conversion rates in the simulation.

For simulating the reactor behaviour with open porous membranes and considering the interactions between reactor and membranes the same control system as before was used but with an oxygen membrane model based on the permeabilities given in Fig. 15 instead of an active controller. The flux through these membranes is driven by the total pressure difference between the reactor and the outside of the membranes. The main parameters for influencing the permeability of real membranes are the pore-sizes, the porosity and the membrane thickness. Because the permeability

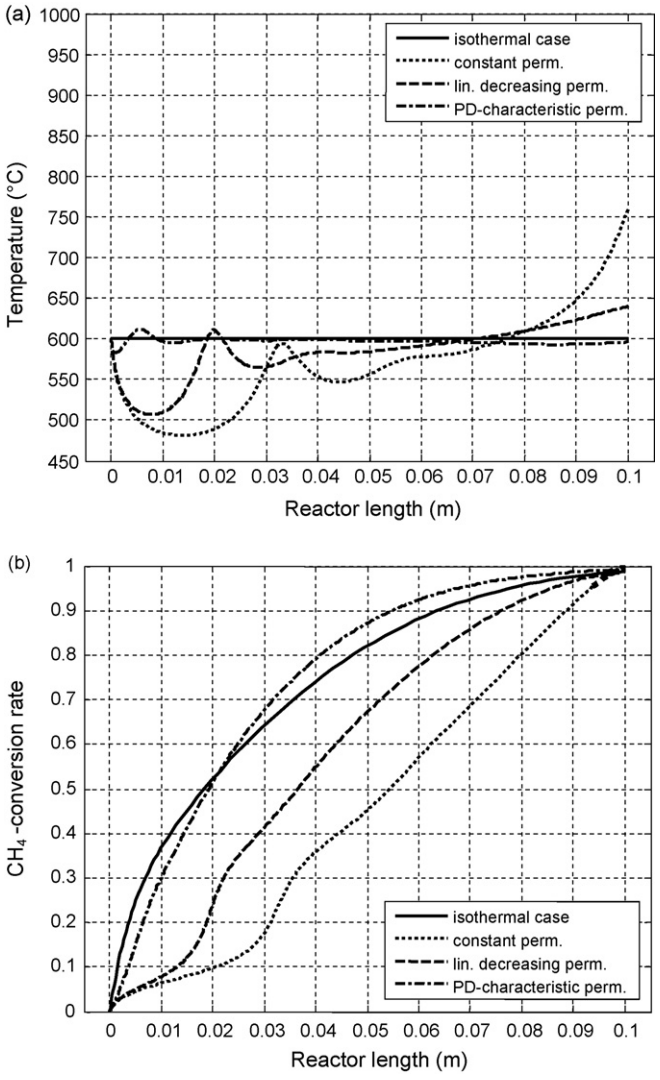

Fig. 16. Temperature (a) and CH_4-conversion (b) profiles for the oxygen feeding through membranes with constant permeability, linear decreasing permeability and with permeability based on PD-controller characteristic, all compared to the isothermal case.

is the parameter of interest and there are many ways for influencing, in the simulations the permeability was used directly. To achieve the PD-optimized oxygen flux more precisely, in this case 10% of the oxygen flux was added to the inlet gases, too. The results from these simulations are given in form of the temperature and CH_4-conversion rate profiles in Fig. 16.

In the case of constant permeability and linear decreasing permeability the same problems occur as already mentioned with the relay control (Fig. 16a), in the entrance region the amount of oxygen is too low and the temperature falls far below the isothermal temperature (480 °C for constant perm. and 506 °C for linear decreasing perm.) and in the outlet region the amount of oxygen is especially with the constant permeability too high and the temperature rises for that case up to 760 °C. In contrast with it, the dash-dotted line representing the optimized membrane is very close to the isothermal case for the temperature profile as well as for the conversion rate profile. As maximum temperature difference only 35 °C was realised in the region of the P-controller but with much slower oscillations. After this the temperature difference remained within a 10 °C region of the isothermal temperature until the end of the reactor. From the conversion rate profile one can observe that what happens in the reactor is similar to the behaviour with the saturation control, meaning that in the outlet region the steam-reforming looses its influence and the water-gas-shift becomes stronger. But as mentioned before this should be no problem and can be advantageous due to the carbon monoxide yield in the reactor outlet.

4. Conclusions

In this investigation a sensitivity analysis of membrane parameters was performed to assess the influence of design parameters on the performance of membrane reactors for autothermal reforming. It could be shown that a prerequisite for optimal performance is to consider the interactions between all functional components of such a reactor and that it cannot be achieved by independent improvements of single components. From the simulations concerning the interactions between hydrogen separation membrane and the reactions in the reformer the following conclusions can be drawn and used as design hints:

- There is a small region in the thickness of the Pd/Ag-layer in which the diffusion through this membrane has much influence on the reactor performance. Above 20 μm the permeation through this membrane is too small and below 400 nm the diffusion is fast enough not to be any more the limitating step of the reactor system.
- Therefore it is not necessary to decrease the thickness under this level of 400 nm with respect to autothermal reforming, but to optimize other objectives like mechanical or thermal stability.

Considering the state of the art technologies for producing hydrogen separation membranes, it could be remarked that the temperature of 600 °C is probably too high for commonly applied membranes. From reported investigations, Pd–Ag-membranes with porous ceramics supports have been successfully tested in regions up to 500 °C [18]. The main problem in this temperature range has been identified to be the different thermal expansion between the materials leading to a loss of the layers adherence. The second aspect is the difficulties related to the deposition of very thin layers of 400 nm on porous supports with high permeation. In technologies currently in use, the pore-sizes of the support decrease strongly with decreasing Pd–Ag-layer and therefore reducing the support's permeability.

However, the main goal of this investigation is to show limits for designing such a membrane from the application point of view. Considering that even with the state of the art technologies the realization of these limits is slightly away, it would be very interesting to develop new technologies attain this.

With respect to oxygen control the following conclusions might be helpful for future membrane design:

- In agreement with other groups the simulations showed that premixing the whole amount of oxygen to the inlet gas leads to high temperature hot-spots shortly after the inlet.
- Membranes with constant permeability and therefore a constant feeding of oxygen can calm these hot-spots, but lead to too low temperatures in the entrance region.
- Linear decreasing permeability in such a membrane has a slight better characteristic but is still far away from the ideal isothermal case.
- We found the best characteristic a membrane that has a similar oxygen flux characteristic as a PD-controller. This could be realized with an exponential decreasing permeability and an additional premixing of oxygen to the inlet gases.

For the realisation of such open porous membranes we have to consider, that there is also a flux in the opposite direction of the oxygen flux due to the diffusion of reactants and especially hydrogen driven by partial pressure differences. Because the effective diffusion is not independent of the convective oxygen flux, this should be no problem for regions with high oxygen fluxes. But to the end of the reactor, where no more oxygen is needed, this can probably lead to a loss of a huge amount of the hydrogen product. Therefore, it is necessary to consider this aspect while producing and characterize such membranes.

However, for both membranes we tried to find limits and optima for designing and with the results of this work it should be a little bit easier to determine the way for future research, what is considering more about mechanical and thermal stability in the case of the hydrogen removal membrane and to produce oxygen membranes with distributed permeability.

Acknowledgements

The funding of the research project by the Deutsche Forschungsgemeinschaft through the Research Training Group PoreNet is gratefully acknowledged.

Appendix A. Reaction model

The reaction system of the autothermal membrane reformer was assumed to be sufficiently precise modelled by three reactions take place in are based on the experimental study of Numaguchi and Kikuchi [20] concerning the steam-reforming and the water gas shift and on the work of de Smet et al. [21] for the methane combustion. They corrected the experimental results by Trimm and Lam [22] with Pt/Al_2O_3 – catalyst to Ni/Al_2O_3 – catalyst, so that we have in all the reactions the kinetic expressions based on Ni. This reaction model was already successfully used and investigated by the work of Tiemersma et al. [5]. The three reactions considered in the model are the steam-reforming of methane (SR)

$$CH_4 + H_2O \leftrightarrow CO + 3\,H_2 \quad (\Delta H_R^0 = 206(\mathrm{kJ/mol}))$$

combustion of methane (MC)

$$CH_4 + 2O_2 \rightarrow CO_2 + 2\,H_2O \quad (\Delta H_R^0 = -36(\mathrm{kJ/mol}))$$

and the water-gas-shift (WGS)

$$CO + H_2O \leftrightarrow CO_2 + H_2 \quad (\Delta H_R^0 = -41(\mathrm{kJ/mol}))$$

The reaction rates can be estimated as follows:

$$r_{MC} = \frac{k_{MCa} p_{CH_4} p_{O_2}}{(1 + K_{CH_4}^{OX} p_{CH_4} + K_{O_2}^{OX} p_{O_2})^2} + \frac{k_{MCb} p_{CH_4} p_{O_2}}{(1 + K_{CH_4}^{OX} p_{CH_4} + K_{O_2}^{OX} p_{O_2})} \tag{A1}$$

$$r_{SR} = \frac{k_{SR}(p_{CH_4} p_{H_2O} - p_{H_2}^3 p_{CO}/K_{eq,SR})}{p_{H_2O}^{1.596}} \tag{A2}$$

$$r_{WGS} = \frac{k_{WGS}(p_{CO} p_{H_2O} - p_{H_2} p_{CO_2}/K_{eq,WGS})}{p_{H_2O}} \tag{A3}$$

with the kinetic rate constants

$$k_{MCa} = 8.11 \times 10^5\ \mathrm{mol/bar^2\ kg_{cat}s} \exp\left(\frac{-86(\mathrm{kJ/mol})}{RT}\right) \tag{A4a}$$

$$k_{MCb} = 6.82 \times 10^5\ \mathrm{mol/bar^2\ kg_{cat}s} \exp\left(\frac{-86(\mathrm{kJ/mol})}{RT}\right) \tag{A4b}$$

$$k_{SR} = 2.62 \times 10^5\ \mathrm{mol/bar^{0.404}\ kg_{cat}s} \exp\left(\frac{-106.9(\mathrm{kJ/mol})}{RT}\right) \tag{A5}$$

$$k_{WGS} = 2.62 \times 10^5\ \mathrm{mol/bar^{0.404}\ kg_{cat}s} \exp\left(\frac{-106.9(\mathrm{kJ/mol})}{RT}\right). \tag{A6}$$

The mass transport limitations (adsorption and desorption of molecules on and off the catalyst) are considered in the estimation of the over-all reaction rates by the adsorption coefficients of an Arrhenius type:

$$K_{CH_4}^{OX} = 0.126\,1/\mathrm{bar} \exp\left(\frac{27.3(\mathrm{kJ/mol})}{RT}\right) \tag{A7}$$

$$K_{O_2}^{OX} = 7.87 \times 10^{-7} 1/\mathrm{bar} \exp\left(\frac{92.8(\mathrm{kJ/mol})}{RT}\right). \tag{A8}$$

The equilibrium constants are only needed for the steam-reforming and the water-gas-shift and can be estimated as follows

$$K_{eq,SR} = p^2 \exp\left(\frac{-\Delta G_{SR}}{RT}\right) \tag{A9}$$

$$K_{eq,WGS} = \exp\left(\frac{-\Delta G_{WGS}}{RT}\right) \tag{A10}$$

Appendix B. Detailed model 1D (DM1D)

As mentioned in the article, we used a second, more detailed model to make sure that the deviation we receive by neglecting the dispersion of mass and heat and by using a different strategy to reach a steady-state (in the FM1D we assumed that we have already steady conditions). This model is given here and several terms are of course the same as in FM1D and therefore already described in the according chapter:

$$\frac{\partial(\varepsilon\rho_g)}{\partial t} + \frac{\partial(\varepsilon\rho_g u)}{\partial z} = \frac{4}{D_R}\sum_i M_i J_i^{Mem} \tag{B1a}$$

$$\frac{\partial(\varepsilon\rho_g u)}{\partial t} + \frac{\partial(\varepsilon\rho_g u^2 + \varepsilon p)}{\partial z} = -\beta\varepsilon\rho_g u + \frac{\partial}{\partial z}\left(\varepsilon\mu_g^* \frac{\partial u}{\partial z}\right) \tag{B1b}$$

$$\frac{\partial(\varepsilon\rho_g\omega_i)}{\partial t} + \frac{\partial(\varepsilon\rho_g u\omega_z)}{\partial z} = \frac{\partial}{\partial z}\left(\rho_g D_i \frac{\partial\omega_i}{\partial z}\right) + (1-\varepsilon)\rho_s M_i \sum_i \nu_{ji} r_i + \frac{4}{D_R} M_i J_i^{Mem} \tag{B1c}$$

$$(\varepsilon\rho_g c_{p,g} + (1-\varepsilon)\rho_s c_s)\frac{\partial(T)}{\partial t} + c_{p,g}\frac{\partial(\varepsilon\rho_g u T)}{\partial z} = \frac{\partial}{\partial z}\left(\lambda_{eff}\frac{\partial T}{\partial z}\right) + (1-\varepsilon)\rho_s \sum_j r_j(-\Delta H_j). \tag{B1d}$$

New in this model are the unsteady terms on the left hand side of all equations and on the right hand side the dispersion terms in the momentum equation, the species equations and in the energy conservation equation.

For describing the viscous flow in the z-direction we assumed, that the gas mixture behaves like an ideal Newtonian fluid and Stoke's hypotheses is true, so that the shear stress reduces to

$$\tau_{zz} = \mu_g^* \frac{\partial u}{\partial z}, \tag{B2}$$

with

$$\mu_g^* \approx \frac{4}{3}\mu_g. \tag{B3}$$

The effective dispersions of mass and heat in porous media can be estimated by a combination of the diffusion coefficients with zero fluid flow and the effects of flow on dispersion as a function of the Peclet number.

$$D_{i,\mathrm{eff}} = \left(1 - \sqrt{1-\varepsilon}\right) D_{i,\mathrm{m}} + \frac{u d_\mathrm{p}}{2} \quad \text{resp.} \tag{B4}$$

$$\frac{\lambda_\mathrm{eff}}{\lambda_\mathrm{g}} = \frac{\lambda_\mathrm{bed}}{\lambda_\mathrm{g}} + \frac{Pe_x}{2} \tag{B5}$$

In these equations $D_{i,\mathrm{m}}$ is the molecular diffusion coefficient of the species i, d_p is a hydraulic parameter e.g. the average pore diameter and Pe_x is the Peclet number estimated with [11].

$$Pe_x = \frac{u \rho_\mathrm{g} c_{\mathrm{p,g}}}{\lambda_\mathrm{g}} X_\mathrm{F} \tag{B6}$$

where $X_\mathrm{F} = F d_\mathrm{p}$ is the effective mixing length and $F = 1{,}15$ for spherical particles. Already in 1970, Zehner and Schlünder [25] presented a model still frequently used to compute the zero flow heat conductivity in porous media which is given here.

$$\frac{\lambda_\mathrm{bed}}{\lambda_\mathrm{g}} = \left(1 - \sqrt{1-\varepsilon}\right)\left(1 + \frac{\lambda_\mathrm{rad}}{\lambda_\mathrm{g}}\right) + \sqrt{1-\varepsilon}\left\{\frac{2}{1 - \lambda_\mathrm{g}/\lambda_\mathrm{s} B} \times \left[\frac{(1-\lambda_\mathrm{g}/\lambda_\mathrm{s})B}{(1-\lambda_\mathrm{g}/\lambda_\mathrm{s}B)^2} \ln\frac{\lambda_\mathrm{s}}{\lambda_\mathrm{g}B} - \frac{B+1}{2} - \frac{B+1}{1-(\lambda_\mathrm{g}/\lambda_\mathrm{s})B}\right] + \frac{1}{(\lambda_\mathrm{g}/\lambda_\mathrm{rad}) + (\lambda_\mathrm{g}/\lambda_\mathrm{s})}\right\} \tag{B7}$$

with

$$B = 1{,}25\left(\frac{1-\varepsilon}{\varepsilon}\right)^{10/9}. \tag{B8}$$

The influence of radiation can approximately expressed as

$$\lambda_\mathrm{rad} = \frac{0.23}{(2/\varepsilon_\mathrm{rad}) - 1}\left(\frac{T}{100}\right)^3 d_\mathrm{p}. \tag{B9}$$

References

[1] L.F. Brown, A comparative study of fuels for on-board hydrogen production for fuel-cell-powered automobiles, Int. J. Hydrogen Energy 26 (2001) 381–397.
[2] C. Palm, P. Cremer, R. Peters, D. Stolten, Small-scale testing of a precious metal catalyst in the autothermal reforming of various hydrocarbon feeds, J. Power Sources 106 (2002) 231–237.
[3] S. Roy, Fluidized bed steam methane reforming with high-flux membranes and oxygen input, Ph.D. Thesis, University of Calgary, Canada, 1998.
[4] M. Dogan, D. Posarac, J. Grace, A.E.M. Adris, C. Jim Lim, Modeling of autothermal steam methane reforming in a fluidized bed membrane reactor, Int. J. Chem. React. Eng. 1 (2003) 1–12.
[5] T.P. Tiemersma, C.S. Patil, M. van Sint Annaland, J.A.M. Kuipers, Modelling of packed bed membrane reactors for autothermal production of ultrapure hydrogen, Chem. Eng. Sci. 61 (2006) 1602–1616.
[6] N.S. Kaisare, J.H. Lee, A.G. Fedorov, Hydrogen generation in a reverse-flow microreactor. Part 1. Model formulation and scaling, AIChE J. 51 (8) (2005) 2254–2264.
[7] N.S. Kaisare, J.H. Lee, A.G. Fedorov, Hydrogen generation in a reverse-flow microreactor. Part 2. Simulation and analysis, AIChE J. 51 (8) (2005) 2265–2272.
[8] F. Galluci, L. Paturzo, A. Basile, A simulation study of the steam reforming of methane in a dense tubular membrane reactor, Int. J. Hydrogen Energy 29 (2004) 611–617.
[9] J.W. Phair, S.P.S. Badwal, Materials for separation membranes in hydrogen and oxygen production and future power generation, Sci. Technol. Adv. Mater. 7 (2006) 792–805.
[10] G. Saracco, H.W.J.P. Neomagus, G.F. Versteeg, W.P.M. van Swaaj, High-temperatures membrane reactors: potential and problems, Chem. Eng. Sci. 54 (1999) 1997–2017.
[11] U. Kürten, Modeling of packed bed membrane reactors: Impact of oxygen distribution on conversion and selectivity in partial oxidation systems, Ph.D. Thesis, University of Twente, The Netherlands, 2003.
[12] V.L. Barrio, G. Schaub, M. Rohde, S. Rabe, F. Vogel, J.F. Cambra, P.L. Arias, M.B. Güemez, Reactor modeling to simulate catalytic partial oxidation and steam reforming of methane. Comparison of temperature profiles and strategies for hot spot minimization, Int. J. Hydrogen Energy 32 (2007) 1421–1428.
[13] M. Kajiwara, U. Shigeyuki, T. Kojima, E. Kikuchi, Hydrogen permeation properties through composite membranes of platinum supported on porous alumina, Catal. Today 56 (2000) 65–73.
[14] V.M. Gryaznov, M.M. Ermilova, N.V. Orekhova, Membrane-catalyst systems for selectivity improvement in dehydrogenation and hydrogenation reactions, Catal. Today 67 (2001) 185–188.
[15] K. Hou, R. Hughes, Preparation of thin and highly stable Pd/Ag composite membranes and simulative analysis of transfer resistance for hydrogen separation, J. Membr. Sci. 214 (2003) 43–55.
[16] S. Tosti, Supported and laminated Pd-based metallic membranes, Int. J. Hydrogen Energy 28 (2003) 1445–1454.
[17] S. Abate, G. Centi, S. Perathoner, F. Frusteri, Enhanced stability of catalytic membranes based on a porous thin Pd film on a ceramic support by forming a Pd–Ag interlayer, Catal. Today 118 (2006) 189–197.
[18] L. Yang, Z. Zhang, B. Yao, X. Gao, Hydrogen permeance and surface states of Pd–Ag/ceramic composite membranes, AIChE J. 52 (8) (2006) 2783–2791.
[19] N.S. Kaisare, J.H. Lee, A.G. Fedorov, Operability analysis and design of a reverse-flow microreactor for hydrogen generation via methane partial oxidation, Ind. Eng. Chem. Res. 44 (2005) 8323–8333.
[20] T. Numaguchi, K. Kikuchi, Intrinsic kinetics and design simulation in a complex reaction network; steam-methane reforming, Chem. Eng. Sci. 43 (1988) 2295–2301.
[21] C.R.H. de Smet, M.H.J.M. de Croon, R.J. Berger, G.B. Marin, J.C. Schouten, Design of adiabatic fixed-bed reactors for the partial oxidation of methane to synthesis gas. Application to production of methanol and hydrogen-for-fuel-cells, Chem. Eng. Sci. 56 (2001) 4849–4861.
[22] D.L. Trimm, C.W. Lam, The combustion of methane on platinum-alumina fibre catalysts. Part 1. Kinetics and mechanism, Chem. Eng. Sci. 35 (1980) 1405–1413.
[23] L.F. Shampine, M.W. Reichelt, The Matlab ODE Suite, SIAM J. Sci. Comput. 18 (1997) 1–22.
[24] O. Schramm, A. Seidel-Morgenstern, Comparing porous and dense membranes for the application in membrane reactors, Chem. Eng. Sci. 54 (1999) 1447–1453.
[25] P. Zehner, E.U. Schlünder, Wärmeleitfähigkeit von Schüttungen bei mäßigen temperaturen, Chem. Eng. Technol. 14 (1979) 933–941.